3.1. Introduction

Frictional losses in a mechanical system are of great concern. For conservation of energy and enhancing the active life of mechanical components, such losses have to be curtailed categorically. Employing lubricants with additional friction modifiers produces encouraging results. An extensive overview of literature proclaims that several types of nanomaterials like nanoparticles, nanosheets, or nanocomposites have been used for the purpose owing to their fast tribo-action.[1-7] Nowadays, carbon-based materials like graphene, fullerene, and carbon nanotubes are the center of attention in this innovative research area.[3-11] From our laboratory, too, carbon microspheres,[12,13] reduced graphene oxide, and their composites with nanoparticles, doped nanoparticles, or nanosheets have been recently documented as tribologically active materials.[14-18] A carbon nitride polymer of high thermal stability possessing graphitic structure g-C_3N_4 with weak van der Waals forces amid the 2D-nanosheets appears to be very influential in the field. Still, it has been seldom studied.[19,20] Zhu et al. have described the antiwear performance of bulk g-C_3N_4 with polyvinylidene difluoride (PVDF).[21] The nanosheets of octadecylamine grafted g-C_3N_4 have been used as antiwear and antifriction lubricant additives by Ajay Kumar and associates.[22] Synergistic friction reduction and wear-resistant properties were found by Xu and co-workers for the composite MoS_2/g-C_3N_4.[23] A nanocomposite of copper nanoparticles with g-C_3N_4 has been studied as a lubricant additive.[24] In the recent past, Wu and his associates have used CuO/g-C_3N_4 for enhancing wear resistance of polyimide composite.[25] They have also evaluated the tribological performance of phenolic coatings with varying percentages of g-C_3N_4.[26] Tribological performance of the hybrid g-

C_3N_4/TiO_2 has been studied by Zhang and his group.[27] Thus, the enhanced tribological activity of functionalized g-C_3N_4 with nanoparticles or nanosheets motivated us to explore the use of zinc oxide for its functionalization since zinc oxide nanoparticles have been widely studied as a tribo-active material.[17,28-30]

Zinc oxide has an open hexagonal crystal structure.[31-33] Doping with different atoms as zinc or oxygen substitutes promotes the formation of defects, which affect the structure and eventually result in improved properties.[34-39] These defects may lead to the formation of slip systems that can change the electronic structure and lower the shear strength; ultimately, tribological properties are enhanced.[38,39] The metal ions like magnesium, copper, and aluminium are known to remarkably improve ZnO activity.[17,40-43] However, doping of ZnO by a substitute of oxygen has been seldom considered. Since nitrogen and oxygen occupy an adjacent position in the periodic table, their size and electronegativity are not widely different. Therefore doping by nitrogen in ZnO will produce the least stress in the lattice.[38] Friction and wear behavior of N-doped ZnO thin films deposited by various methods have been recently put on record.[38,39] Besides nanoparticles, nanorod morphology also has yielded promising results in tribology; for example, ZnO, TiO_2, MnO_2, CuS, Fe_2O_3, Fe_3O_4, and Al_2O_3 nanorods are well-known for their friction-reducing properties.[44-52] Khatri et al.[53] reported improved lubricity of copper oxide nanorods over nanoparticles due to rolling and sliding effects. Motivated by these findings, it appeared fascinating to prepare nanorods.

Thus, N-doped ZnO nanorods were prepared,[54] and their tribological activity was evaluated. Since a hybrid of magnesium doped-ZnO nanoparticles with reduced graphene

oxide was reported to produce excellent results,[17,40,41] it compelled us to use N-doped ZnO nanorods for functionalization of tribologically active g-C_3N_4 anticipating significant advancement in the activity. Accordingly, the hybrid N-doped ZnO/g-C_3N_4 was synthesized. The tribological activity of the nanorods, nanosheets, and hybrid was appraised on a four-ball lubricant tester under ASTM D4172 and ASTM D5183 conditions.

3.2. Experimental Section

3.2.1 Materials

In the current work, Analytical Reagent grade chemicals procured from Merck India were used throughout.

3.2.2. Synthesis of additives

3.2.2.1. Preparation of N-doped ZnO nanorods

The synthesis of N-ZnO nanorods was carried out by the hydrothermal method.[54] For N-doped ZnO preparation, 4 mL liquid ammonia was added to the reaction mixture of (1.2 g) zinc acetate and 20 mL ethylenediamine in 15 mL of ethanol. Ethylenediamine provides a basic environment to yield zinc hydroxide, which interacts with ammonia to produce zinc ammine complex, $[Zn(NH_3)_4]^{2+}$.[55] The reaction mixture was heated in a Teflon autoclave at 200 °C for 24 h. The zinc ammine complex formed in the reaction mixture acts as a precursor for nitrogen source to form N-doped zinc oxide nanorods.[55] A white precipitate was collected by centrifugation and washed several times with water, followed by ethanol, and dried at 60 °C.

3.2.2.2 Preparation of g-C_3N_4 nanosheets

The g-C_3N_4 powder was prepared by heating melamine.[56] Melamine (5g) was kept in an alumina crucible with a lid and calcined at 550 °C for 4 h in a muffle furnace. When the crucible came down to room temperature, the sample was taken out and milled to give a g-C_3N_4 powder. The g-C_3N_4 powder was ultrasonicated in 100 mL of 50% alcohol-water mixture for 3-4 h. The obtained colloidal dispersion was centrifuged for 15 min at 4000 RPM for sedimentation of the bigger particles. The supernatant solution was collected; the solvent was evaporated and dried to get g-C_3N_4 nanosheets. The yield of g-C_3N_4 nanosheets was found to be 25%.

3.2.2.3. Preparation of Hybrid N-ZnO/g-C_3N_4

N-ZnO nanorods (200 mg) and g-C_3N_4 nanosheets (300 mg) were dispersed separately in ethanol and sonicated for 1h at approximately 50 °C. The dispersions were assorted by stirring ceaselessly. Sonication of the mixture at 70 °C produced light yellow material. After filtration, the product was dried and kept in a microwave oven for 2 to 3 min at 700 W. At the end, a light-yellow hybrid material of nanostructured N-ZnO with lamellar g-C_3N_4 of nanometer length scale, was obtained.[16,17]

A schematic representation for the procedure of synthesis of hybrid N-ZnO/g-C_3N_4 is shown in Scheme 3.1.

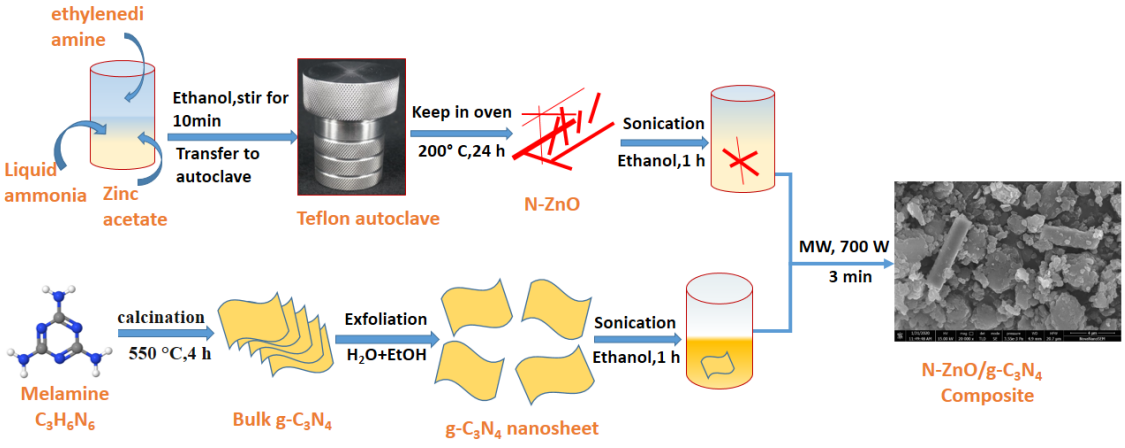

Scheme 3.1. Schematic synthesis of hybrid N-ZnO/g-C_3N_4

3.2.3. Sample preparation

Test samples of different concentrations in the PO, 0.00, 0.10, 0.15, 0.20 and 0.25% w/v were prepared via 1 h sonication at room temperature. The tribological tests were performed at an optimized concentration, i.e., 0.15% w/v in base oil.

3.3. Results and Discussion

3.3.1. Structural and morphological studies of N-doped ZnO, g-C_3N_4 and the hybrid N-doped ZnO/g-C_3N_4

The techniques SEM/HR-SEM, TEM/HR-TEM, XRD, FT-IR, UV/visible, and XPS were used to study the investigated additives. For examining the morphology of N-doped ZnO, g-C_3N_4, and N-doped ZnO/g-C_3N_4, HR-SEM images were taken and are illustrated in Figure 3.1a, 1b, and 1c, respectively. As evident in Figure 3.1a, N-doped ZnO shows the morphology of nanorods.[52] The nanorods as-formed are not uniform in size and diameter. The diameter and the length of the as-formed nanorods lie between 200 nm-6 µm and 3µm-30µm, respectively. As reported, temperature, heating rate, and reaction time show a pronounced effect on the morphology and dimensions of the nanorods.[54] In

Figure 3.1b, arbitrarily piled fluffy nanosheets of g-C_3N_4 are clearly visible.[57] The lateral size of nanosheets lies in the range 200 nm to 1300 nm with a thickness of 12-18 nm as measured by image J software. Figure 3.1c divulges nanorods of N-doped ZnO embellishing g-C_3N_4 nanosheets. The EDX analysis of the hybrid, Figure 3.1d, provides the presence of elements carbon, nitrogen, oxygen, and zinc, confirming the hybrid formation. EDX spectra of N-doped ZnO and g-C_3N_4 are given in Figure 3.2a and 2b.

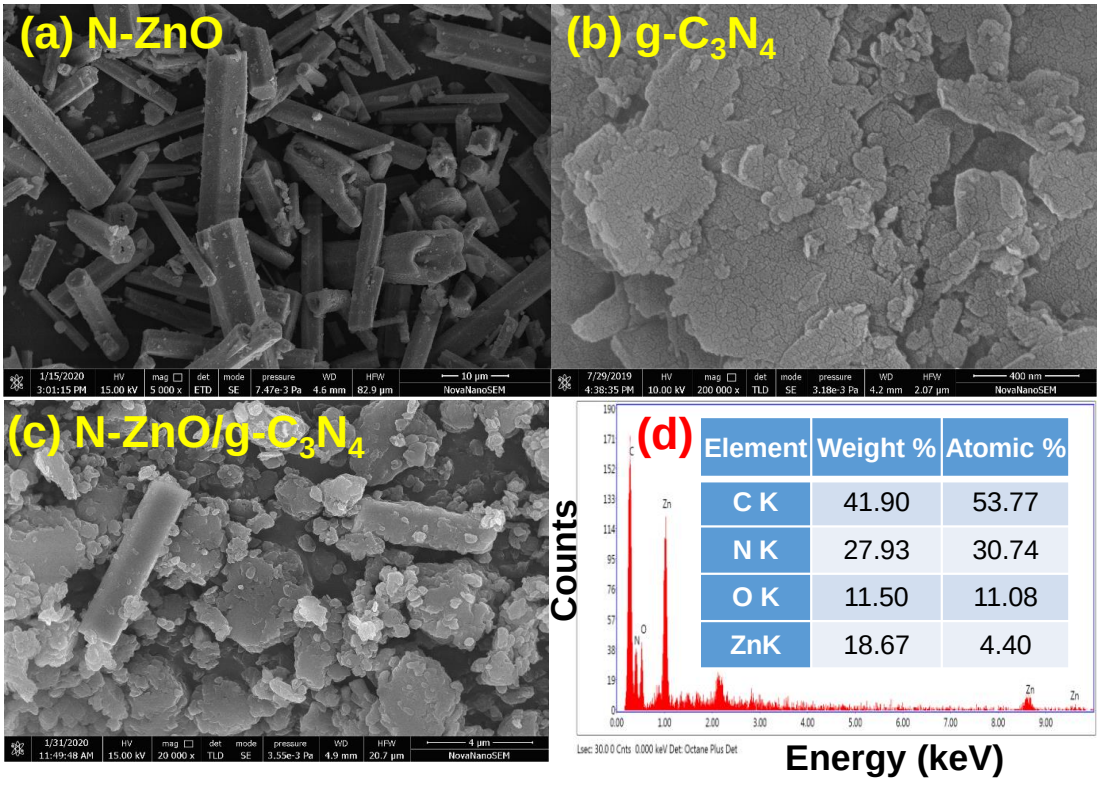

Figure 3.1. HR-SEM images of (a) N-ZnO, (b) g-C_3N_4, (c) N-ZnO/g-C_3N_4 and (d) EDX spectrum of N-ZnO/g-C_3N_4

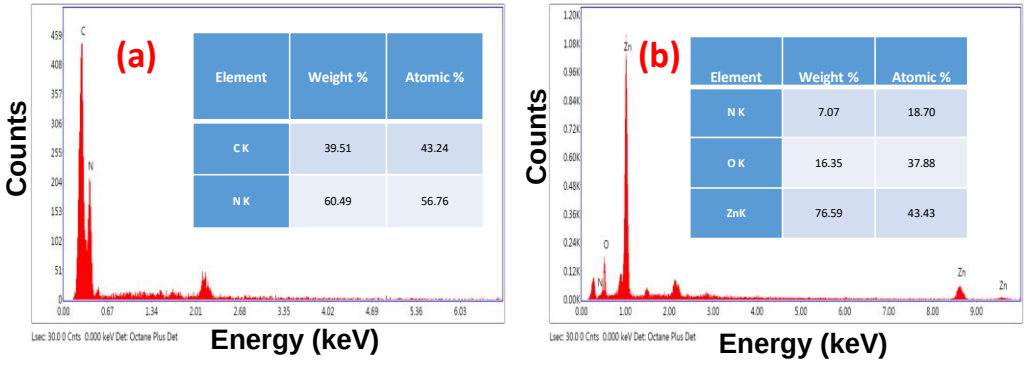

Figure 3.2. EDX spectrum of (a) g-C_3N_4 (b) N-ZnO

For a more exquisite perception of the morphology, TEM images of g-C_3N_4, N-doped ZnO, and N-doped ZnO/g-C_3N_4 have also been recorded and are presented in Figure 3.3a, 3b, and 3c, respectively. The lamellar structure of g-C_3N_4 can be clearly seen in Figure 3.3a. In Figure 3.3b, an N-doped ZnO rod can be seen. The cross-section of the nanorods is not circular but polygonal; edges and ridges are well apparent in the SEM images. The HR-TEM image of g-C_3N_4 nanosheets is displayed in Figure 3.3a_1. The interplanar spacing of the nanosheet corresponding to the (002) plane was found as 0.32 nm.[57,58] The HR-TEM image of N-doped ZnO is shown in Figure 3.3b_1. Figure 3.3c delineates the anchored nanorods on g-C_3N_4 nanosheets. The HR-TEM image of the hybrid, Figure 3.3c_1, reveals the interplanar spacing of the N-ZnO as 0.24 nm correlating with (101) plane.[57,58] Further, the lattice fringes spacing of the g-C_3N_4, corresponding to (002) plane, has increased to 0.35 nm in the hybrid. The increase of interplanar spacing of (002) plane in g-C_3N_4 emphasizes that N-doped ZnO nanorods have interacted well with the nanosheets of g-C_3N_4.[16] These nanorods have acted as separators amid the nanosheets and controlled the re-piling of the nanosheets.[50,51] The selected area diffraction pattern (SAED) of the hybrid is indicative of substantial crystallinity.

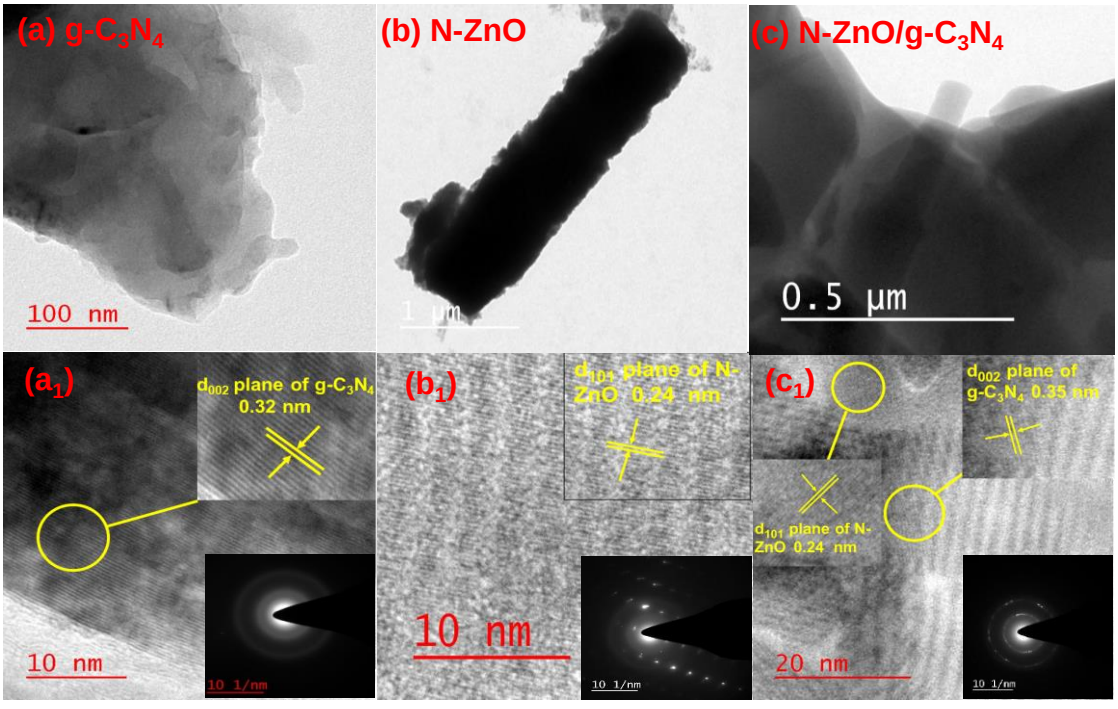

Figure 3.3. TEM images of (a) g-C_3N_4, (b) N- ZnO, (c) N- ZnO/g-C_3N_4, and HR-TEM images of g-C_3N_4 (a_1), N-ZnO (b_1) and N-ZnO/g-C_3N_4 (c_1). The inset in (a_1, b_1, and c_1) provides the SAED pattern of the additives.

Figure 3.4a portrays XRD patterns of N-doped ZnO, g-C_3N_4, and N-doped ZnO/g-C_3N_4. In the diffraction pattern of g-C_3N_4, an intense peak at 27.5° is identified for (002) plane corresponding to interplanar stacking.[57,58] This peak shifts slightly towards the lower angle in the hybrid. The XRD pattern of N-ZnO nanorods followed JCPDS No. 36-1451. It could be convincingly indexed for the hexagonal wurtzite ZnO.[57,58] Absence of any additional peak other than those of ZnO confirms single-phase. Therefore, nitrogen is doped in the ZnO crystal lattice. N-doped ZnO peaks undergo a marginal shift towards lower value in the hybrid, probably due to the significant interaction of the nanorod with the nanosheets.[57] Moreover, the intensity of the peaks is faintly reduced in the hybrid.

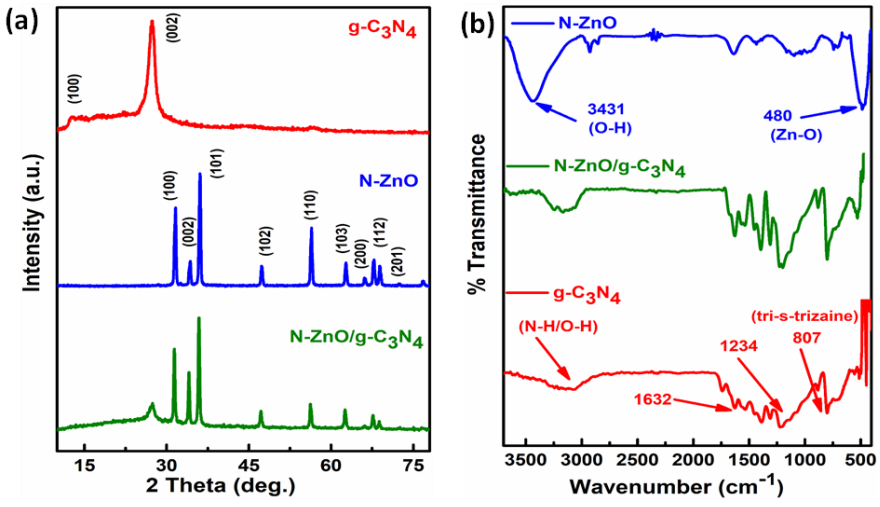

Figure 3.4. (a) XRD patterns of as-prepared g-C_3N_4, N-ZnO, and N-ZnO/g-C_3N_4, (b) IR of g-C_3N_4, N-ZnO, and N-ZnO/g-C_3N_4

The IR spectra of the additives are shown in Figure 3.4b. The FTIR spectrum of N-doped ZnO exhibits a peak around 480 cm^{-1} for the bending mode of Zn-O, which is observed at a similar position in the hybrid.[57,58] The spectrum of g-C_3N_4 is characterized by the presence of s-triazine ring vibrations for breathing mode at 807 cm^{-1}.[57,58] The C-N and C=N stretching modes of g-C_3N_4 could be identified at 1234 and 1632 cm^{-1}, respectively.[57,58] A broadband appearing in the range 3100-3300 cm^{-1} is ascribed to the stretching mode of vibrations for N-H, and O-H bonds of primary/secondary amines, and water, respectively.[57,58] The presence of characteristic peaks of g-C_3N_4 in the hybrid verifies the continuation of its basic structure in the hybrid. The lowering (redshift) of these stretching frequencies in the composite indicates extended conjugation with N-doped ZnO.[57,58] Thus, N-doped ZnO has interacted significantly with g-C_3N_4 in the composite.

The X-ray Photoelectron Spectroscopy was employed to identify the chemical states of the constituent elements in the composite N-ZnO/g-C_3N_4. Figure 3.5 shows the deconvoluted core level spectra of C 1s, N 1s, O 1s, and Zn 2p using peak fit the software. Figure 3.5a clearly portrays core level spectra of C 1s showing peaks with binding energies 286.3 and 287.9 eV corresponding to singly and doubly bonded carbon in the N-C=N, respectively.[57,58] A peak with binding energy 284.1 eV could be ascribed to adventitious carbon at the surface of the composite.[57,58] Figure 3.5b exhibits two peaks in the O 1s spectrum at binding energy 530.2 and 531.2 eV. Figure 3.5c shows two peaks in the N1s spectrum at 397.4 eV and 398.7 eV assignable to Zn-N (anionic nitrogen) and sp^2 nitrogen (C-N=C).[57,58] The 2p core-level spectrum of Zn displayed in Figure 3.5d divulges two peaks at binding energies 1021.6 and 1044.8 eV characteristic of Zn $2p_{3/2}$ and Zn $2p_{1/2}$, respectively.[57,58] The XPS spectra of N-ZnO and g-C_3N_4 remains unaffected in the composite[57,58] indicating that there is no chemical interaction between them.

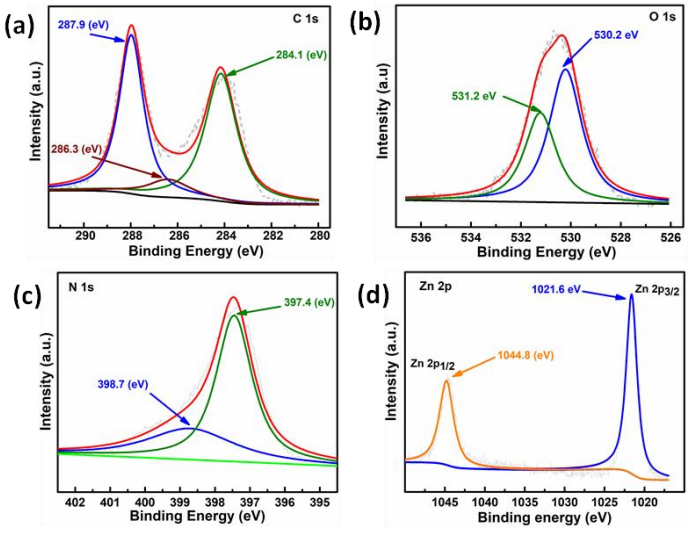

Figure 3.5. Deconvoluted XPS spectra of (a) C 1s core-level spectra, (b) O 1s core-level spectra, (c) N 1s core level spectra, (d) Zn 2p core-level spectra

3.3.2. Tribological Properties

3.3.2.1. Determination of Stability of Nanofluids

The stability of dispersions of the additives in base lube is of significant concern for their tribological applications. Use was made of UV/visible spectroscopy for the said purpose. The dispersions of additives containing optimized concentration were prepared by ultrasonication and then diluted 10 times with base lube. The absorbance values of diluted dispersions were recorded in the range of 300-800 nm at 0, 12, 24, and 48 h. The relative absorbance of the dispersions has been plotted against settling time and depicted in Figure 3.6a. The minimum decrease in relative absorbance is indicative of the maximum stability of the dispersion. Accordingly, dispersion of hybrid material appears to have maximum stability, followed by N-doped ZnO, and then g-C_3N_4 shows the least stability. For increasing the dispersibility graphene nanosheets, functionalization is meaningful[59,60] as nanoparticles/nanorods separate the nanosheets from repiling and decrease their agglomeration mutually by steric stabilization.[61] As a consequence of decreased agglomeration, dispersity is enhanced.

The absorbance of the hybrid dispersion initially and after 12, 24, and 48 h is presented in the inset of Figure 5a. As evident from the figure, there is an abysmal decline in absorbance amidst 48 h. The base lube and its blends with the additives have been photographed in the beginning, and after 48 h. These photographs are presented in Figure 3.6b.

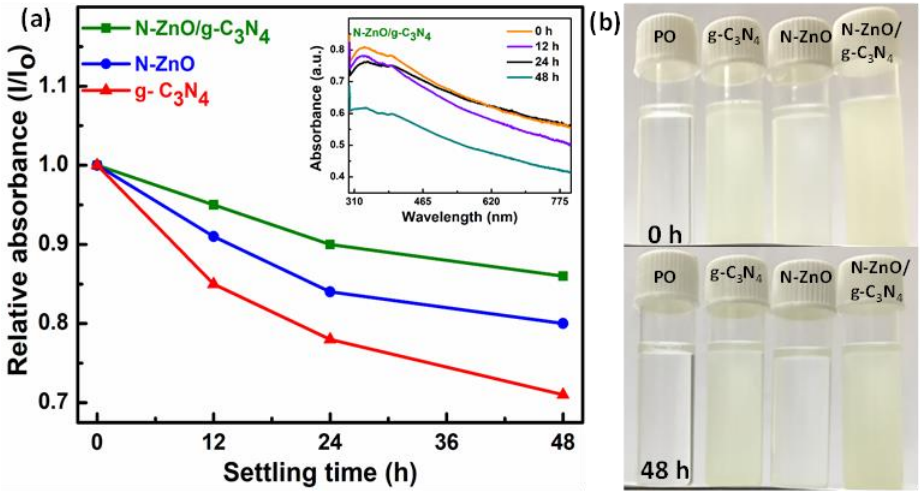

Figure 3.6. (a) Dispersion stabilities of base oil containing g-C_3N_4, N-doped ZnO, and N-ZnO/g-C_3N_4 by UV-vis spectrophotometry, (b) Optical photographs of the additives dispersed in base oil at 0 and 48 h

3.3.2.2.Optimization of concentration of the additives

Since the concentration is the most critical variable for determining the efficiency of the additives, it has to be optimized first. For optimization, blends of varying concentrations of the additives, 0.00, 0.10, 0.15, 0.20, and 0.25% w/v in paraffin oil, were tested under ASTM D4172 conditions, and the corresponding values of mean wear scar diameter (MWD) are shown in Figure 3.7a. In general, MWD values diminish remarkably for all the tested concentrations of all the s compared to plain paraffin oil. Thus, all the tested additives behave as antiwear additives at all the tested concentrations; however, efficiencies are widely different. At all the tested concentrations, the relative performance of the hybrid appears to be the best among the three additives as the MWD is least in the case of hybrid compared to the other two additives. The N-doped ZnO occupies the next place in performance, while g-C_3N_4 shows the weakest performance out of the tested

additives. In general, the MWD has decreased from the concentration of 0.10% w/v till 0.20% w/v, but beyond that, it increases, except in g-C_3N_4 where MWD increases after 0.15% w/v. Thus, 0.20% of w/v has been considered as the optimized concentration for conducting the tests.

3.3.2.3. Antiwear and Anti-friction Properties

ASTM D4172 test was conducted to determine the antiwear efficiency of different additives in paraffin oil. The test results are delineated in Figure 3.7b in the form of a bar diagram where both the coefficient of friction (COF) and MWD data have been shown simultaneously. As discernible from the Figure, MWD 0.735 mm for the plain oil has declined in every case; g-C_3N_4 (12%), N-doped ZnO (28.51%), and N-ZnO/g-C_3N_4 (37.24%). The decrease in MWD is directly related to antiwear efficiency. At 0.20% w/v there is 15.42% reduction in MWD for ZnO nanoparticles[17] while 28.51% for N-doped ZnO. Thus, N-doping in ZnO has enhanced the activity, performed better than ZnO nanoparticles. Thus, around 13% enhancement in activity has been noted in going from ZnO nanoparticles to N-doped ZnO nanorods. The hybrid is more efficient than N-doped ZnO, which, in turn, is better than g-C_3N_4. The average COF value of base lube, 0.079, shows concurrent order as that of antiwear efficiency, COF reduction g-C_3N_4 (40.51%), N-doped ZnO (46.84%), and N-ZnO/g-C_3N_4 (57.14%).

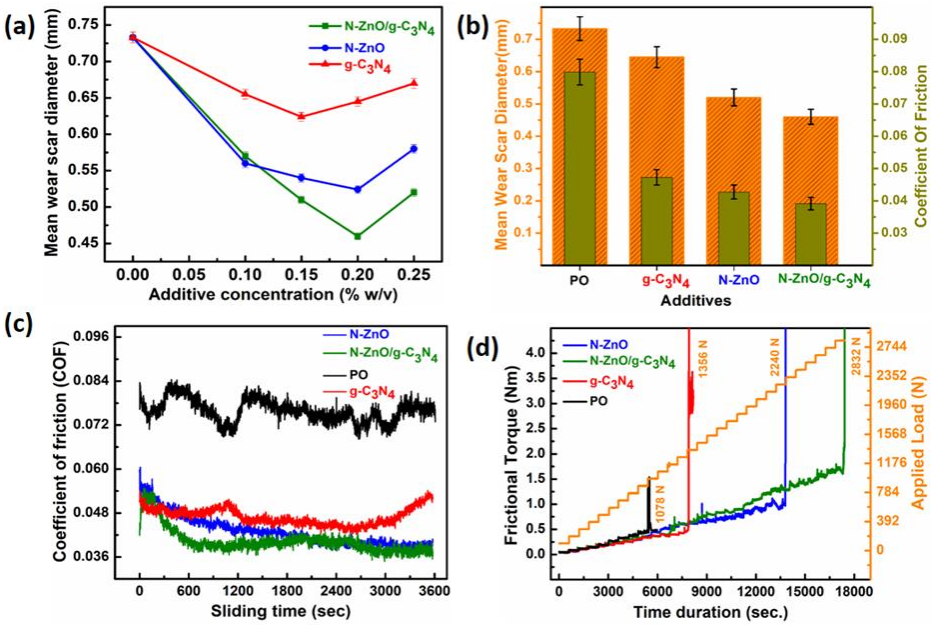

Figure 3.7. (a) Optimization of concentration of different additives and variation of tribological parameters of paraffin oil with and without optimized concentration (0.20% w/v) of various additives under ASTM D4172 conditions (b) mean wear scar diameter and the average coefficient of friction (c) coefficient of friction as a function of sliding time (d) Variation of frictional torque as a function of stepwise loading and time for PO in absence and presence of different additives under ASTM D5183 conditions

Figure 3.7c depicts the variation of COF of paraffin oil without and with additives against time. Undoubtedly, the COF values for blank oil are throughout considerably higher with varying amplitude than its blends with the additives. The COF seems to be reduced and stabilized in the presence of additives. Initially, the COF is somewhat higher in every case because of the absence of tribofilm. After some time, the tribofilm is formed, and COF is minimized consistently. Here the trend similar to antiwear and antifriction behavior is again observed.

3.3.2.4. Load Bearing Capacity

A load ramp test has been conducted under ASTM D5183 conditions. Initially, to complete the running-in period, the test has been conducted following the conditions; 392 N load, 600 RPM, temperature 75 °C, and 60 min using an optimized concentration of the additives. Further, the steady-state test is continued by subsequent addition of 98 N load at 10 min intervals until the abrupt increase of frictional torque occurs, resulting in the seizure of the surface of balls. The results are described in Figure 3.7d. In the presence of base lube, a sudden rise in frictional torque occurs at the load 1078 N. Consequently, the proximal surfaces get seized, and the corresponding load is termed as the seizure load. At this load, physically, the tribofilm is disrupted, and the lubricant can no longer bear the load. The gap between frictional torque values between base lube and its blends with additives has enlarged with a simultaneous increase of load and time. As notable from the Figure, seizure load (SL) obtained for different admixtures; g-C_3N_4 (1356 N), N-doped ZnO (2240 N), and N-doped ZnO/g-C_3N_4 (2832 N) reveals the load-bearing capacity of the tested additives. Thus, like wear and friction-reducing tendencies, the remarkable load-bearing ability is noted for the hybrid.

3.3.2.5. Frictional Power Loss

According to the equation (3.1), the frictional power loss (P) was calculated for paraffin oil in the absence and the presence of the tested additives.

$$P = 221 \times \mu \text{ (W)} \quad (3.1)$$

Where, μ = coefficient of friction

$$1 \text{ kWh} = 3.6 \text{ MJ} \quad (3.2)$$

Table 3.1. Frictional power reduction in the presence of blends of optimized concentration, 0.2% (w/v) of different additives in paraffin oil

S.N.	Additives	Power consumption (MJ)	Reduction in Power consumption	% Reduction in Power consumption
1.	PO	0.0628	____	____
2.	g-C_3N_4	0.0376	0.0252	40.2
3.	N-ZnO	0.0339	0.0289	46.0
4.	N-ZnO/g-C_3N_4	0.0311	0.0317	50.5

As described in Table 3.1, maximum power consumption (0.0628 MJ) was perceived for plain paraffin oil without any additive. For its admixtures with different additives, there is a remarkable cutback in power consumption, 0.0376 MJ for g-C_3N_4, 0.0339 MJ for N-ZnO, and 0.0311 MJ for the hybrid. Thus, maximum energy saving occurs in the case of the hybrid.

3.3.3. Morphological Studies of the Worn Surface

The surface techniques, AFM and SEM, have assisted in revealing the morphology of the worn surface on the tested steel ball after conducting the antiwear test. The SEM micrographs of the surface lubricated with base lube and its blends with additives containing the optimized concentration (0.20% w/v) are collected in Figure 3.8a.

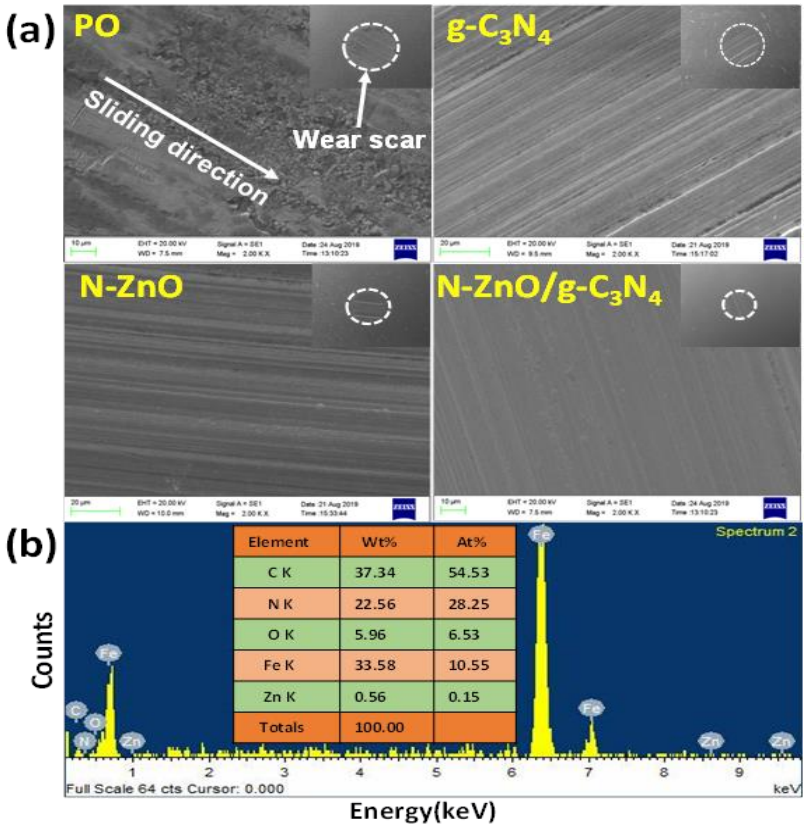

Figure 3.8. (a) SEM micrographs of the tribofilm formed on the worn steel surfaces at 2.00 KX magnification lubricated with paraffin oil in the presence and absence of different additives (0.2% w/v) for 60 min test duration at 392N applied load, inset showing wear scar surfaces at higher magnification 100 KX (b) EDX spectrum of worn steel surface lubricated with N-ZnO/g-C_3N_4 hybrid

For plain paraffin oil, SEM image divulges a crumpled surface due to dreadful scratches. The upgraded surface is definitely visible in the presence of the admixtures. The relative magnitude of the surface advancement validates the above-discussed tribological data. The MWD values given in the inset of micrographs correlate very well with the smoothness of the surface. As might be expected, outstanding evenness of the surface is

perceived when oil blended with hybrid is used for lubrication. EDX analysis of the wear track, Figure 3.8b, acknowledges the presence of all the constituent elements of the additives, indicating strongly adsorbed additives on the ball surface. EDX spectra of worn surfaces of g-C_3N_4 and N-doped ZnO are given in Figure 3.9a and b.

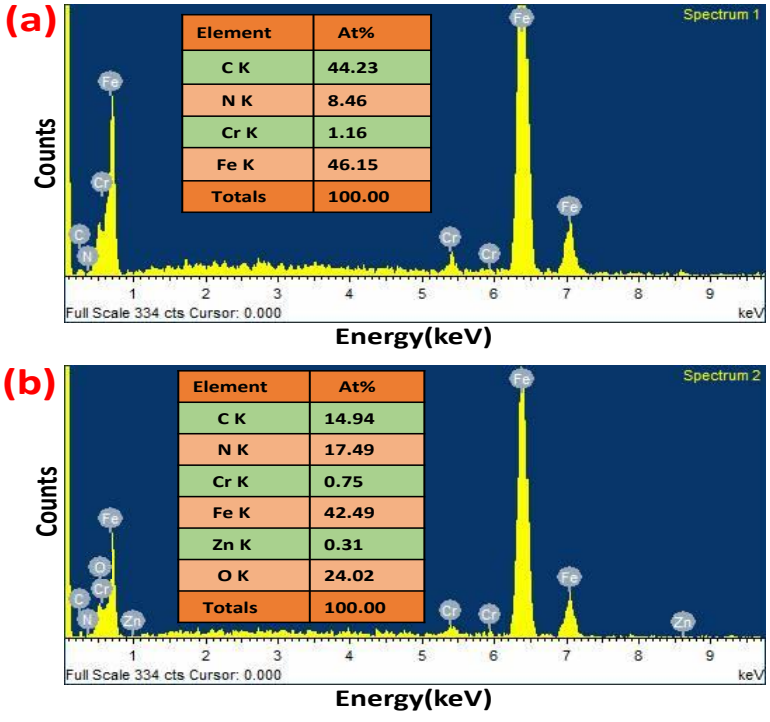

Figure 3.9. EDX spectrum of worn surfaces of (a) g-C_3N_4 (b) N-ZnO

Furthermore, contact mode AFM was employed to quantify surface roughness of steel ball lubricated with base lube without and with additives after the antiwear test. The *2D* and *3D* AFM images of the wear track and data related to the surface roughness, line roughness (Rq), and area roughness (Sq) are provided in Figure 3.10. The Rq and Sq values undergo enormous reduction from base oil to the additives. As per expectation, minimum roughness is observed when hybrid is used as an additive. Other roughness parameters like Sa, Ra, Sy, Ry, Sp, Rp, Sv, Rv, Sm, and Rm have been provided in Table 3.2.

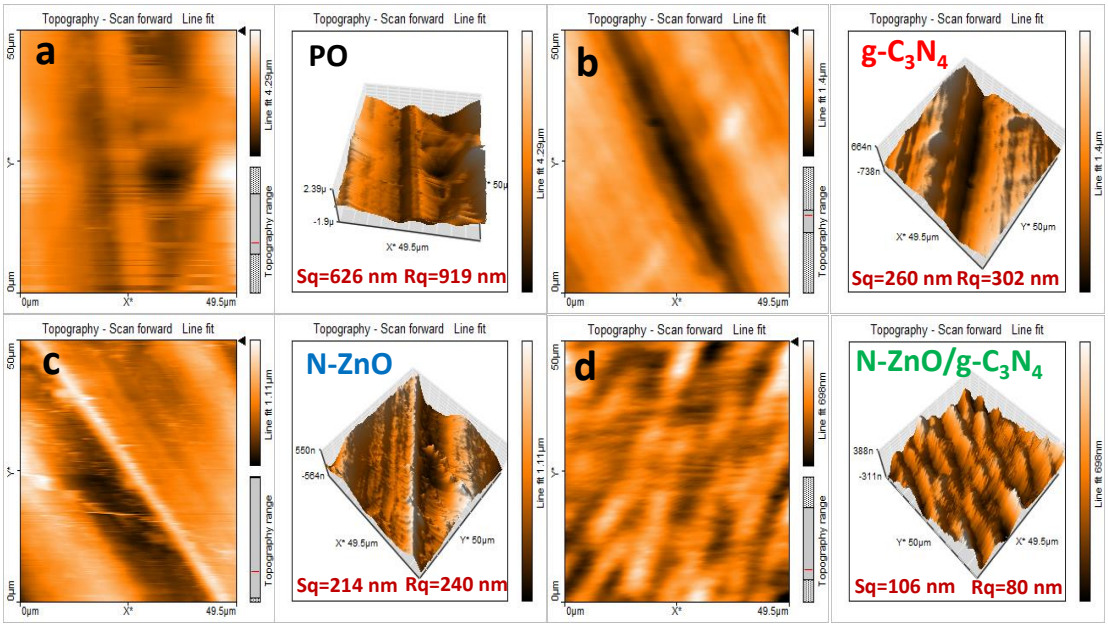

Figure 3.10. *2D* and *3D* AFM images of the worn steel surface lubricated with the optimized concentration of different additives in paraffin oil for 60 min test duration at 392 N applied load: (a) Paraffin oil, (b) g-C_3N_4, (c) N-doped ZnO and (d) N-ZnO/g-C_3N_4

Table 3.2. Surface roughness parameters obtained from the digital processing software of AFM (Nanosurf-basic Scan-2) for different additives after the antiwear test.

Surface roughness parameter	**Sq (nm)**	**Rq (nm)**	**Sa (nm)**	**Ra (nm)**	**Sy (nm)**	**Ry (nm)**	**Sp (nm)**	**Rp (nm)**	**Sv (nm)**	**Rv (nm)**	**Sm (pm)**	**Rm (pm)**
PO	626	919	488	771	4363	3255	2611	2060	-1752	-1195	129	-129
g-C_3N_4	260	302	207	259	1307	1000	610	316	-697	-684	217	-109
N-ZnO	214	240	176	188	1272	969	749	573	-523	-396	106	-214
N-ZnO/g-C_3N_4	106	80	84	69	945	300	520	144	-425	-157	126	-183

(Where, S = Areal roughness, and R = Linear roughness parameters).

Sq = root mean square height, Rq = root mean square line

Sa = Arithmetical mean height, Ra = Arithmetic mean line

Sy = Maximum height of the surface, Ry = Maximum height of the profile

Sp = Maximum peak height**,** Rp = Maximum profile peak height

Sv = Maximum valley depth, Rv = Maximum profile valley depth

Sm = Mean width area, Rm = Mean width line

3.3.4. Analysis of Tribofilm by XPS

The XPS spectra of the wear track lubricated with hybrid were recorded after the antiwear test to identify chemical states of the individual elements of the tribofilm formed *in situ*. The deconvoluted core level spectra of C 1s, O 1s, N 1s, Zn 2p, and Fe 2p are portrayed in Figures 3.11a, b, c, d, and e utilizing peak fit software.

The position of the peaks in C1s, N1s, O1s, and Zn 2p spectra is almost the same as obtained in the XPS spectra of the hybrid before the test. A little shift in the peaks indicates that zinc oxide nanorod might have tribosinterized at the tribo surfaces. Besides, the iron of the steel surface is oxidized to ferric oxide, as revealed by the presence of peaks in the Fe 2p spectrum for Fe $2p_{3/2}$ (710.5 eV) and Fe $2p_{1/2}$ (724.2 eV).[12-17] Thus, based on the characterization of tribofilm by XPS spectra, it may be inferred that tribofilm is made up of the adsorbed organic contents of g-C_3N_4, N-ZnO, and tribochemically oxidized Fe_2O_3.

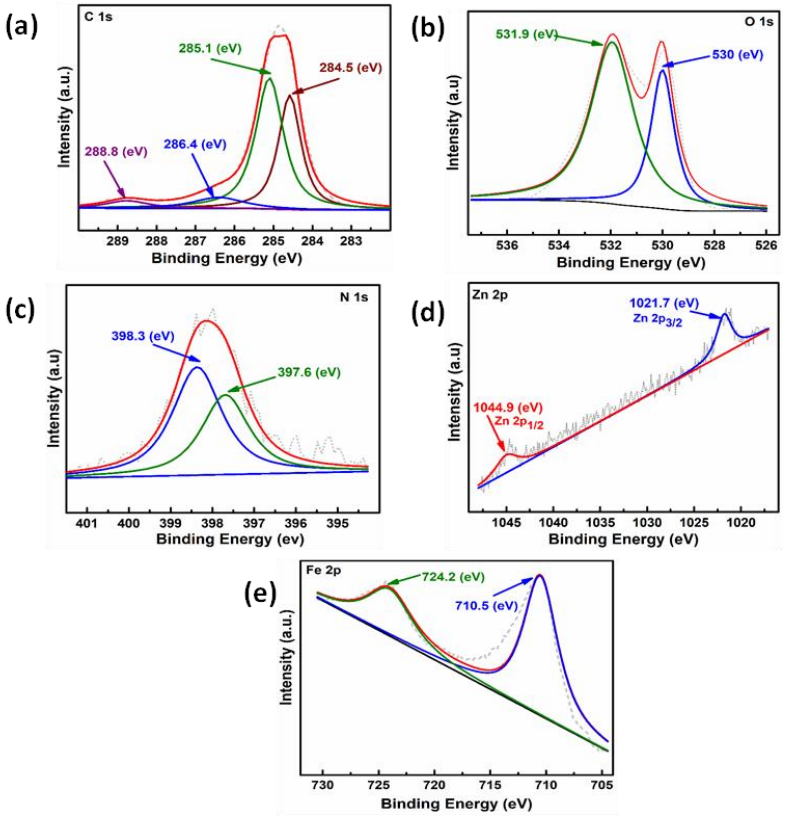

Figure 3.11. Deconvoluted XPS spectra of the tribofilm formed on the steel surface lubricated with N-ZnO/g-C_3N_4 nanocomposite under ASTM D4172 test conditions: (a) C 1s spectra, (b) O 1s spectra, (c) N 1s spectra, (d) Zn 2p spectra and (e) Fe 2p spectra.

3.3.5. Proposed Mechanism of Lubrication

An overview of the obtained results and their discussion reveals that the efficacy of the tested additives is associated with their tenacity to the interacting surfaces, which ultimately advances to the construction of tribofilm *in situ* under prevailing conditions of the tribological test. It is, indeed, the tribofilm that bears the load. The characteristics of tribofilm, composition, adherence, and endurance are crucial in explaining the resultant efficiency of an additive. Zinc oxide nanoparticles are well known for their tribological activity; doping with nitrogen has enhanced the lubrication due to the formation of

defects.[38,39] The defects are known to form slip systems, which affect the electronic structure, and eventually, shear strength is lowered.[38,39] Nanoparticles may behave like ball bearings and can be easily trapped between asperities. Nanorods being comparatively harder, are not easily trapped.[62] In general, the nanorods are known to perform much better than nanoparticles due to predominant rolling and sliding actions.[53,62] The higher aspect ratio (length/breadth ratio) of nanorods provides enhanced tribological characteristics.[53]

Assuredly, the robust polymeric layered structure of g-C_3N_4 has promoted ease in sliding motion.[16,22,24] The magnificent tribological performance of the hybrid N-doped ZnO/g-C_3N_4 towards reducing wear, friction, and enhancing seizure load may be entrusted to mutualistic interaction between the nanorods and nanosheets.[50] The nanosheets and nanorods have mutually cooperated in controlling their agglomeration.[50] The nanorods lying between nanosheets have segregated the sheets and prevented them from being restacked.[44,45,50] The sliding motion has smoothened further by rolling action of nanorods between the tribo surfaces or nanosheets.[49,53,62-64] The nanorods have cooperated in enhancing lubricity by healing the contacting surfaces via the process of tribosinterization where the tiny fissures formed on the tribo-surfaces are filled effectively by unidimensional nanorods.[49,50,63,64] Thus, a mixed effect of all the above mechanisms has led to the superb performance of the hybrid. The schematic diagram of lubrication is given for a proper understanding of the mechanism of lubrication in Figure 3.12.

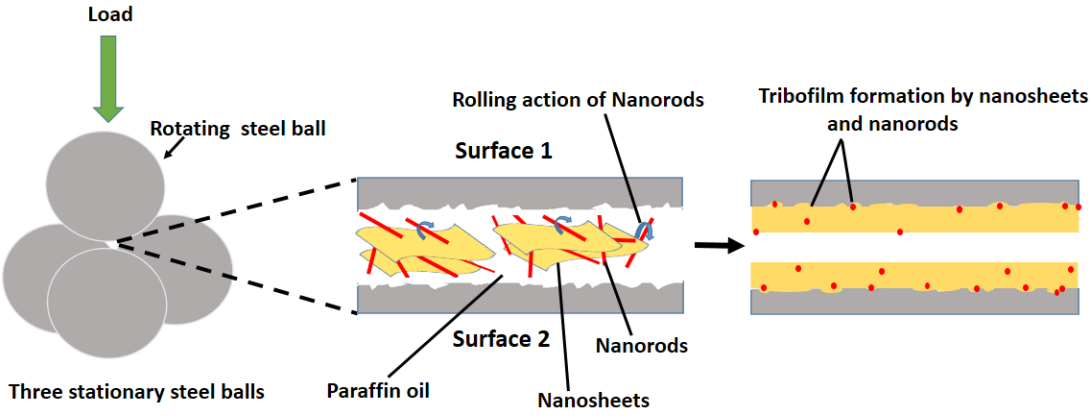

Figure 3.12. The schematic diagram for the proposed mechanism of lubrication

3.4. Conclusions

The g-C_3N_4 nanosheets were prepared by heating melamine, followed by ultrasonication. The hydrothermal method was used to prepare N-doped ZnO nanorods. The hybrid of nanorods and nanosheets was prepared by ultrasonication. The techniques HR-SEM with EDX, TEM/HR-TEM, FT-IR, and powder XRD were applied to characterize the as-prepared nanomaterials. Nanorods morphology was identified for N-doped ZnO, which is ascribed to experimental conditions, time, temperature, and heating rate, etc. Morphology of hybrid reveals the nanorods spread between nanosheets and bonded to them via weak physical interactions. The hybrid dispersion in paraffin oil was stable even after 48 h, as indicated by absorbance values recorded using UV/visible spectroscopy. Examination of antiwear/antifriction activity (ASTM D4172 test) and load-bearing capacity (ASTM D5183 test) of the synthesized nanomaterials on four-ball tester at the optimized concentration 0.20% w/v reveals the order as given - g-C_3N_4 < N-doped g-C_3N_4 < N-doped ZnO << N-ZnO/g-C_3N_4.

No doubt, synergy between nanorods with nanosheets has worked efficiently in the hybrid. SEM and AFM studies of the wear pathway support the above statement. XPS studies of the wear track divulge that the tribofilm is composed of ZnO, adsorbed g-C_3N_4, and Fe_2O_3. The enhanced nanorod lubrication by a combined effect of tribosinterization and rolling mechanisms. Doping of nitrogen in ZnO has yielded defects, which further has upgraded lubrication. Nanorods were acting as separators between nanosheets controlling their agglomeration. The unparalleled tribo-activity of the hybrid, N-doped ZnO/g-C_3N_4, is unequivocally due to the synergistic interactions between nanorods and nanosheets. Thus, the hybrid proves its candidacy as aspiring wear and friction modifier for lubrication systems.

3.4. References

(1) Uflyand, I. E.; Zhinzhilo, V. A.; Burlakova, V. E. Metal-containing nanomaterials as lubricant additives: State-of-the-art and future development. *Friction* **2019**, *7*, 93-116.

(2) Kumar, B.; Verma, D. K.; Kavita.; Rastogi, R. B. Tribological activity of ionic liquid stabilized calcium-doped ceria nanoparticles. *P. I. Mech. Eng. J-J Eng.* **2020**, 1-8.

(3) Zhao, J.; Huang, Y.; Li, Y.; Gao, T.; Dou, Z.; Mao, J.; Wang, H.; He, Y.; Li, S.; Luo. J. Superhigh-exfoliation graphene with a unique two-dimensional (2D) microstructure for lubrication application. *Appl. Surf. Sci.* **2020**, *513*, 145608-145617.

(4) Zhang, J.; Xu, Q.; Gao, L.; Ma, T.; Qiu, M.; Hu, Y.; Wang, H.; Luo, J. A molecular dynamics study of lubricating mechanism of graphene nanoflakes embedded in Cu-based nanocomposite. *Appl. Surf. Sci.* **2020**, *511*, 145620-145628.

(5) Liu, L.; Zhou, M.; Jin, L.; Li, L.; Mo, Y.; Su, G.; Li, X.; Zhu, H.; Tian, Y. Recent advances in friction and lubrication of graphene and other 2D materials: mechanisms and applications. *Friction* **2019**, *7*, 199-216.

(6) Paul, G.; Hirani, H.; Kuila, T.; Murmu, N. C. Nanolubricants dispersed with graphene and its derivatives: an assessment and review of the tribological performance. *Nanoscale* **2019**, *11*, 3458-3483.

(7) Sun, J.; Du, S. Application of graphene derivatives and their nanocomposites in tribology and lubrication: a review. *RSC Adv.* **2019**, *9*, 40642-40661.

(8) Turan, M. E.; Sun, Y.; Akgul, Y. Mechanical, tribological and corrosion properties of fullerene reinforced magnesium matrix composites fabricated by semi powder metallurgy. *J. Alloys Compd*. **2018**, *740*, 1149-1158.

(9) Wang, Z.; Ren, R.; Song, H.; Jia, X. Improved tribological properties of the synthesized copper/carbon nanotube nanocomposites for rapeseed oil-based additives. *Appl. Surf. Sci*. **2018**, *428*, 630-639.

(10) Sun, Z.; Cheng, X. Investigation of carbon nanotube-containing film on silicon substrates and its tribological behaviour. *Appl. Surf. Sci*. **2015**, *355*, 272-278.

(11) Song, W.; Yan, J.; Ji, H. Tribological Study of the SOCNTs@ MoS_2 Composite as a lubricant additive: Synergistic effect. *Ind. Eng. Chem. Res.* **2018**, *57*, 6878-6887.

(12) Kumar, B.; Verma, D. K.; Shukla, N.; Singh, A. K.; Rastogi, R. B. Ionic liquid stabilized Ag@ C composite for improvement of triboactivity. *J. Mol. Liq*. **2020**, *307*, 113012-113021.

(13) Kumar, B.; Verma, D. K.; Singh, A. K.; Kavita.; Shukla, N.; Rastogi, R. B. Nanohybrid Cu@ C: synthesis, characterization and application in enhancement of lubricity. *Compos. Interfaces* **2019**, 777-794.

(14) Shukla, N.; Verma, D. K.; Singh, A. K.; Kumar, B., Kavita; Rastogi, R. B. Ternary Composite of Methionine-Functionalized Graphene Oxide, Lanthanum Doped Yttria Nanoparticles, and Molybdenum Disulfide Nanosheets for Thin Film Lubrication. *ACS Appl. Nano Mater.* **2020**, *3*, 8012-8026

(15) Verma, D. K.; Kuntail, J.; Kumar, B.; Singh, A. K.; Shukla, N.; Kavita.; Sinha, I.; Rastogi, R. B. Amino Borate-Functionalized Reduced Graphene Oxide Further

Functionalized with Copper Phthalocyanine Nanotubes for Reducing Friction and Wear. *ACS Appl. Nano Mater.* **2020**, *3*, 5530-5541.

(16) Verma, D. K.; Shukla, N.; Kumar, B.; Singh, A. K.; Shahu, K.; Yadav, M.; Rhee, K. Y.; Rastogi, R. B. Synergistic Tribo-Activity of Nanohybrids of Zirconia/Cerium-Doped Zirconia Nanoparticles with Nano Lamellar Reduced Graphene Oxide and Molybdenum Disulfide. *Nanomaterials* **2020**, *10*, 707-726.

(17) Verma, D. K.; Kumar, B.; Kavita.; Rastogi, R. B. Zinc oxide-and magnesium-doped zinc oxide-decorated nanocomposites of reduced graphene oxide as friction and wear modifiers. *ACS Appl. Mater. Interfaces* **2018**, *11*, 2418-2430.

(18) Jaiswal, V.; Umrao, S.; Rastogi, R. B.; Kumar, R.; Srivastava, A. Synthesis, characterization, and tribological evaluation of TiO_2-reinforced boron and nitrogen co-doped reduced graphene oxide based hybrid nanomaterials as efficient antiwear lubricant additives. *ACS Appl. Mater. Interfaces*. **2016**, *8*, 11698-11710.

(19) Groenewolt, M.; Antonietti, M. Synthesis of g-C_3N_4 nanoparticles in mesoporous silica host matrices. *Adv. Mater*. **2005**, *17*, 1789-1792.

(20) Wang, X.; Maeda, K.; Thomas, A.; Takanabe, K.; Xin, G.; Carlsson, J. M.; Domen, K.; Antonietti, M. A metal-free polymeric photocatalyst for hydrogen production from water under visible light. *Nat. Mater*. **2008**, *8*, 76–80.

(21) Zhu, L.; Wang, Y.; Hu, F.; Song, H. Structural and friction characteristics of g-C_3N_4/PVDF composites. *Appl. Surf. Sci.* **2015**, *345*, 349-354.

(22) Kumar, A.; Thakre, G. D.; Arya, P. K.; Jain, A. K. 2D Structured Nano-Sheets of Octadecylamine Grafted Graphitic-Carbon Nitride (g-C_3N_4) as Lubricant Additives. *Macromol. Symp*. **2017**, *376*, 1700009-1700015.

(23) XUa, Z. D.; XINa, J. B.; FANa, R. X.; Wang, K.; Yang, J. A simple approach to fabricate g-C_3N_4/MoS_2 nanocomposite and its application as a lubricant additive. *Dig. J. Nanomater. Bios.* **2018**, *13*, 731-741.

(24) Yang, J.; Zhang, H.; Chen, B.; Tang, H.; Li, C.; Zhang, Z. Fabrication of the g-C_3N_4/Cu nanocomposite and its potential for lubrication applications. *RSC Adv*. **2015**, *5*, 64254-64260.

(25) Wu, L.; Zhang, Z.; Yang, M.; Yuan, J.; Li, P.; Guo, F.; Men, X. Facile synthesis of CuO/g-C_3N_4 hybrids for enhancing the wear resistance of polyimide composite. *Eur. Polym. J.* **2019**, 116, 463-470.

(26) Wu, L.; Zhang, Z.; Yang, M.; Yuan, J.; Li, P.; Guo, F.; Men, X. One-step synthesis of g-C_3N_4 nanosheets to improve tribological properties of phenolic coating. *Tribol. Int*. **2019**, 132, 221-227.

(27) Zhang, F.; Tang, G.; Xu, J.; Li, C. Solvothermal preparation and tribological performance of g-C_3N_4/TiO_2 hybrids as oil-based lubricant additives. *Micro Nano Lett*. **2019**, *14*, 1355-1360.

(28) Wu, L.; Zhang, Y.; Yang, G.; Zhang, S.; Yu, L.; Zhang, P. Tribological properties of oleic acid-modified zinc oxide nanoparticles as the lubricant additive in poly-alpha olefin and diisooctyl sebacate base oils. *RSC Adv.* **2016**, *6*, 69836-69844.

(29) Prasad, S. V.; McDevitt, N. T.; Zabinski, J. S. Tribology of tungsten disulfide-nanocrystalline zinc oxide adaptive lubricant films from ambient to 500 °C. *Wear* **2000**, *237*, 186-196.

(30) Battez, A. H.; Rico, J. F.; Arias, A. N.; Rodriguez, J. V.; Rodriguez, R. C.; Fernandez, J. D. The tribological behaviour of ZnO nanoparticles as an additive to PAO6. *Wear* **2006**, *261*, 256-263.

(31) Wahab, R.; Kim, Y. S.; Lee, K.; Shin, H. S. Fabrication and growth mechanism of hexagonal zinc oxide nanorods via solution process. *J. Mater. Sci.* **2010**, *45*, 2967-2973.

(32) Chen, Y.; Yu, R.; Shi, Q.; Qin, J.; Zheng, F. Hydrothermal synthesis of hexagonal ZnO clusters. *Mater. Lett*. **2007**, *61*, 4438-4441.

(33) Bitenc, M.; Drazic, G.; Orel, Z. C. Characterization of crystalline zinc oxide in the form of hexagonal bipods. *Cryst. Growth Des.* **2010**, *10*, 830-837.

(34) Phan, D. T.; Chung, G. S. Effects of defects in Ga-doped ZnO nanorods formed by a hydrothermal method on CO sensing properties, Sensor. *Actuat. B-Chem*. **2013**, *187*, 191-197.

(35) Mao, C.; Fang, L.; Zhang, H.; Li, W.; Wu, F.; Qin, G.; Ruan, H.; Kong, C. Effect of B doping on optical, electrical properties and defects of ZnO films. *J. Alloys Compd*. **2016**, *676*, 135-141.

(36) Lee, H. B.; Ginting, R. T.; Tan, S. T.; Tan, C. H.; Alshanableh, A.; Oleiwi, H. F.; Yap, C. C.; Jumali, M. H. H.; Yahaya, M. Controlled defects of fluorine-incorporated ZnO nanorods for photovoltaic enhancement. *Sci. Rep*. **2016**, *6*, 32645-32655.

(37) Pal, B.; Sarkar, D.; Giri, P. K. Structural, optical, and magnetic properties of Ni doped ZnO nanoparticles: correlation of magnetic moment with defect density. *Appl. Surf. Sci*. **2015**, *356*, 804-811.

(38) Olofinjana, B.; Mbamara, U. S.; Ajayi, O.; Lorenzo-Martin, C.; Obiajuuwa, E. I.; Ajayi, E. O. B. Tribological behavior of N-doped ZnO thin films by metal organic chemical vapor deposition under lubricated contacts. *Friction* **2017**, *5*, 402-413.

(39) Mbamara, U. S.; Olofinjana, B.; Ajayi, O. O.; Lorenzo-Martin, C.; Obiajunwa, E. I.; Ajayi, E. O. B. Friction and wear behavior of nitrogen-doped ZnO thin films deposited via MOCVD under dry contact. *Int. J. Eng. Sci. Technol*. **2016**, *19*, 956-963.

(40) Rastogi, R. B.; Kumar, D. Synthesis, characterization, and tribological evaluation of SDS-stabilized magnesium-doped zinc oxide ($Zn_{0.88}Mg_{0.12}O$) nanoparticles as efficient antiwear lubricant additives. *ACS Sustain. Chem. Eng*. **2016**, *4*, 3420-3428.

(41) Kalyani.; Jaiswal, V.; Rastogi, R. B.; Kumar, D. The investigation of different particle size magnesium-doped zinc oxide ($Zn_{0.92}Mg_{0.08}O$) nanoparticles on the lubrication behavior of paraffin oil. *Appl. Nanosci*. **2017**, *7*, 275-281.

(42) Charde, S. J.; Sonawane, S. S.; Rathod, A. P.; Sonawane, S. H.; Shimpi, N. G.; Parate, V. R. Copper-doped zinc oxide nanoparticles: influence on thermal, thermo mechanical, and tribological properties of polycarbonate. *Polym. Compos*. **2018**, *39*, E1398-E1406.

(43) Lin, L. Y.; Jeong, M. C.; Kim, D. E.; Myoung, J. M. Micro/nanomechanical properties of aluminum-doped zinc oxide films prepared by radio frequency magnetron sputtering. *Surf. Coat. Technol*. **2006**, *201*, 2547-2552.

(44) Fei, J.; Luo, D.; Huang, J.; Zhang, C.; Duan, X.; Zhang, L. Growth of aligned ZnO nanorods on carbon fabric and its composite for superior mechanical and tribological performance. *Surf. Coat. Technol.* **2018**, *344*, 433-440.

(45) Luo, D.; Fei, J.; Zhang, C.; Li, H.; Zhang, L.; Huang, J. Optimization of mechanical and tribological properties of carbon fabric/resin composites via controlling ZnO nanorods morphology. *Ceram. Int.* **2018**, *44*, 15393-15401.

(46) Zhang, J.; Zhang, J. Surfactant inducing phase change of ZnO nanorods to low friction. *Tribol. Lett.* **2013,** *49*, 77-83.

(47) Lin, Z.; Jia, X.; Yang, J.; Li, Y.; Song, H. Interfacial modification and tribological properties of carbon fiber grafted by TiO_2 nanorods reinforced novel depolymerized thermosetting composites. *Compos. Part A Appl. Sci. Manuf.* **2020**, 105860-105870.

(48) Kumar, N.; Bhaumik, S.; Sen, A.; Shukla, A. P.; Pathak, S. D. One-pot synthesis and first-principles elasticity analysis of polymorphic MnO_2 nanorods for tribological assessment as friction modifiers. *RSC Adv.* **2017**, *7*, 34138-34148.

(49) Chen, L.; Zhu, D. Preparation and tribological properties of unmodified and oleic acid-modified CuS nanorods as lubricating oil additives. *Ceram. Int.* **2017**, *43*, 4246-4251.

(50) Song, H. J.; Jia, X. H.; Li, N.; Yang, X. F.; Tang, H. Synthesis of α-Fe_2O_3 nanorod/graphene oxide composites and their tribological properties. *J. Mater. Chem.* **2012**, *22*, 895-902.

(51) Liu, C.; Yan, H.; Chen, Z.; Yuan, L.; Liu, T. Enhanced tribological properties of bismaleimides filled with aligned graphene nanosheets coated with Fe_3O_4 nanorods. *J. Mater. Chem. A* **2015**, *3*, 10559-10565.

(52) Qiang, H.; Wang, T.; Qu, H.; Zhang, Y.; Li, A.; Kong, L. Tribological and rheological properties of nanorods–Al_2O_3 as additives in grease. *P. I. Mech. Eng. J-J Eng*. **2019**, *233*, 605-614.

(53) Gusain, R.; Khatri, O.P. Ultrasound assisted shape regulation of CuO nanorods in ionic liquids and their use as energy efficient lubricant additives. *J. Mater. Chem. A* **2013,** *1*, 5612-5619.

(54) Varghese, N.; Panchakarla, L. S.; Hanapi, M.; Govindaraj, A.; Rao, C. N. R. Solvothermal synthesis of nanorods of ZnO, N-doped ZnO and CdO. *Mater. Res. Bull.* **2007**, *42*, 2117-2124.

(55) Kobayashi, R.; Kishi, T.; Katayanagi, Y.; Yano, T; Matsushita, N. Fabrication of nitrogen-doped ZnO nanorod arrays by hydrothermal synthesis and ambient annealing. *RSC advances*, **2018**, *8*, 23599-23605.

(56) Jo, W. K.; Lee, J. Y.; Selvam, N. C. S. Synthesis of MoS_2 nanosheets loaded ZnO-g-C_3N_4 nanocomposites for enhanced photocatalytic applications. *Chem. Eng. J.* **2016**, *289*, 306-318.

(57) Kong, J. Z.; Zhai, H. F.; Zhang, W.; Wang, S. S.; Zhao, X. R.; Li, M.; Li, H.; Li, A. D.; Wu, D. Visible light-driven photocatalytic performance of N-doped ZnO/g-C_3N_4 nanocomposites. *Nanoscale Res. Lett.* **2017**, *12*, 1-10.

(58) Kumar, S.; Baruah, A.; Tonda, S.; Kumar, B.; Shanker, V.; Sreedhar, B. Cost-effective and eco-friendly synthesis of novel and stable N-doped ZnO/g-C_3N_4 core-shell nanoplates with excellent visible-light responsive photocatalysis. *Nanoscale* **2014**, *6*, 4830-4842.

(59) Bai, G.; Wang, J.; Yang, Z.; Wang, H.; Wang, Z.; Yang, S. Preparation of a highly effective lubricating oil additive–ceria/graphene composite. *RSC Adv.* **2014**, *4*, 47096-47105.

(60) Zhou, Q.; Huang, J.; Wang, J.; Yang, Z.; Liu, S.; Wang, Z.; Yang, S. Preparation of a reduced graphene oxide/zirconia nanocomposite and its application as a novel lubricant oil additive. *RSC Adv.* **2015**, *5*, 91802-91812.

(61) Yu, W.; Xie, H. A review on nanofluids: preparation, stability mechanisms, and applications. *J. Nanomater.* **2012**, *2012*, 1-17.

(62) Akbulut, M.; Belman, N.; Golan, Y; Israelachvili, J. Frictional properties of confined nanorods. *Adv. Mater.* **2006**, *18*, 2589-2592.

(63) Yang, J.; Yao, H.; Liu, Y.; Zhang, Y. Synthesis and tribological properties of WSe_2 nanorods. *Nanoscale Res. Lett.* **2008**, *3*, 481-485.

(64) Zhang, L. L.; Tu, J. P.; Wu, H. M.; Yang, Y. Z. WS_2 nanorods prepared by self-transformation process and their tribological properties as additive in base oil. *Mater. Sci. Eng. A.* **2007**, *454*, 487-491.